UDC 551.515.21:551.509.313

PRELIMINARY RESULTS FROM AN ASYMMETRIC MODEL OF THE TROPICAL CYCLONE

RICHARD A. ANTHES, STANLEY L. ROSENTHAL, and JAMES W. TROUT

National Hurricane Research Laboratory, Environmental Research Laboratories, NOAA, Miami, Fla.

ABSTRACT

A three-layer primitive equation model of an isolated stationary tropical cyclone is constructed. The major difference between this and previously published models is the elimination of the assumption of circular symmetry. The release of latent heat by organized cumulus convection is parameterized by use of techniques previously shown to give realistic results in symmetrical models. In particular, the total release of heat in a vertical column is given by the horizontal convergence of water vapor in the Ekman layer and the vertical distribution of the heating follows the proposals made by Kuo. In the preliminary calculation reported on here, water vapor content is not forecast but, rather, is treated implicitly as was the case for the earlier circularly symmetric models.

The results show that the model reproduces many observed features of the three-dimensional tropical cyclone. Realistic portrayals of spiral rainbands and the strongly asymmetric structure of the outflow layer are obtained. The kinetic energy budget of the model compares favorably with empirical estimates and also shows the loss of kinetic energy due to truncation errors to be very small.

Large-scale horizontal asymmetries in the outflow are found to play a significant role in the radial transport of vorticity during the mature stage and are of the same magnitude as the transport by the mean circulation.

In agreement with empirical studies, the outflow layer of the model storm shows substantial areas of negative absolute vorticity and anomalous winds.

1. INTRODUCTION

Axisymmetric numerical models have simulated the life cycle of tropical cylcones with a large degree of realism (Ooyama 1969; Yamasaki 1968*a*, 1968*b*; Rosenthal 1970*b*). They have also yielded valuable insight into hurricane dynamics, energetics, and the important problem of parameterizing the latent heat released in organized cumulus convection. With this background, and with ever increasing computer capability, it is not premature to begin the study of the asymmetric features of the hurricane. Among the more notable of these are the upper tropospheric outflow layer, the rainbands, hurricane motion, and interactions between the hurricane and nearby synoptic systems.

Incorporation of all of these features into a single numerical model is an extremely ambitious goal that will require much further investigation. The model developed here represents an isolated stationary vortex and appears to be the logical first step beyond the axisymmetric models. For computational economy, we have limited the model to three vertical levels, a coarse horizontal resolution of 30 km, and a relatively small domain of 435-km radius. The results, nevertheless, are encouraging and appear to justify further effort.

Parallel investigations of our group are concerned with the design of grids with variable horizontal resolution (Anthes 1970*c*, Koss 1971). These will allow us to achieve increases in resolution near the hurricane center as well as in the size of the computational domain, with only moderate increase in the cost of computation. The very difficult problem of linking a large-scale forecast model with a moving high-resolution hurricane model will be investigated in the near future.

2. DESIGN OF THE MODEL

A. BASIC EQUATION

The equations of motion in the σ-coordinate system (Phillips 1957) are

$$\frac{\partial p^*u}{\partial t}=-\frac{\partial p^*u^2}{\partial x}-\frac{\partial p^*uv}{\partial y}-p^*\frac{\partial \dot{\sigma}u}{\partial \sigma}+fvp^* -p^*\frac{\partial \phi}{\partial x}-RT\frac{\partial p^*}{\partial x}+F_H(u)+F_V(u) \quad (1)$$

and

$$\frac{\partial p^*v}{\partial t}=-\frac{\partial p^*vu}{\partial x}-\frac{\partial p^*v^2}{\partial y}-p^*\frac{\partial \dot{\sigma}v}{\partial \sigma}-fup^* -p^*\frac{\partial \phi}{\partial y}-RT\frac{\partial p^*}{\partial y}+F_H(v)+F_V(v). \quad (2)$$

Here, x and y are east-west and north-south Cartesian coordinates on an f-plane. The symbols u and v denote velocity components in the x- and y-directions, respectively; p^* is surface pressure; $\sigma=p/p^*$ where p is the pressure; and $\dot{\sigma}$ is the vertical velocity in the σ-system. The symbol ϕ denotes the geopotential of a σ-surface, T is temperature, and R is the gas constant for dry air. The Coriolis parameter, f, is assigned a value appropriate to approximately 20°N ($5\times10^{-5}s^{-1}$). The terms F_H and F_V represent effects produced by horizontal and vertical eddy diffusivity of horizontal momentum, respectively, and are discussed later.

The continuity and thermodynamic equations are given by

$$\frac{\partial p^*}{\partial t}=-\frac{\partial p^*u}{\partial x}-\frac{\partial p^*v}{\partial y}-\frac{\partial p^*\dot{\sigma}}{\partial \sigma} \quad (3)$$

and

$$\frac{\partial p^*T}{\partial t}=-\frac{\partial p^*uT}{\partial x}-\frac{\partial p^*vT}{\partial y}-\frac{p^*\partial\dot{\sigma}T}{\partial\sigma}+\frac{RT\omega}{c_p\sigma}+\frac{p^*}{c_p}\dot{Q}+F_H(T) \quad (4)$$

where $\dot{Q}$ is the diabatic heating per unit mass, c_p is the specific heat at constant pressure, and $\omega=dp/dt$ is related to $\dot{\sigma}$ by

$$\omega=p^*\dot{\sigma}+\sigma\frac{dp^*}{dt}. \quad (5)$$

$F_H(T)$ represents the lateral diffusion of heat due to the presence of subgrid-scale eddies. In the σ-system, the hydrostatic equation may be written

$$\frac{\partial\phi}{\partial\sigma}=-\frac{RT}{\sigma}. \quad (6)$$

Equations (1) through (6) are identical to those employed by Smagorinsky et al. (1965) for general circulation studies. Since this preliminary calculation does not contain an explicit water vapor cycle, there are seven dependent variables (u, v, p^*, T, ϕ, ω, and $\dot{\sigma}$). The vertical sum of eq (3) is used to compute $\partial p^*/\partial t$ and provides the seventh equation needed to complete the set. Water vapor is treated implicitly in a fashion similar to that used in some symmetric models (Yamasaki 1968*a*, 1968*b*; Rosenthal 1969). The details are given later.

B. STRUCTURE OF THE MODEL

The vertical structure of the model is shown by figure 1A. The atmosphere is divided into upper and lower layers of equal pressure depth and a thinner Ekman boundary layer. The information levels, k, for the dynamic and thermodynamic variables (fig. 1A) are staggered according to the scheme used by Kurihara and Holloway (1967).

The horizontal mesh (fig. 1B) is rectangular with a uniform spacing of 30 km. The lateral boundary points approximate a circle, and all boundary points are contained between radii of 450 and 435 km. All variables are defined at all grid points on the σ-surfaces.

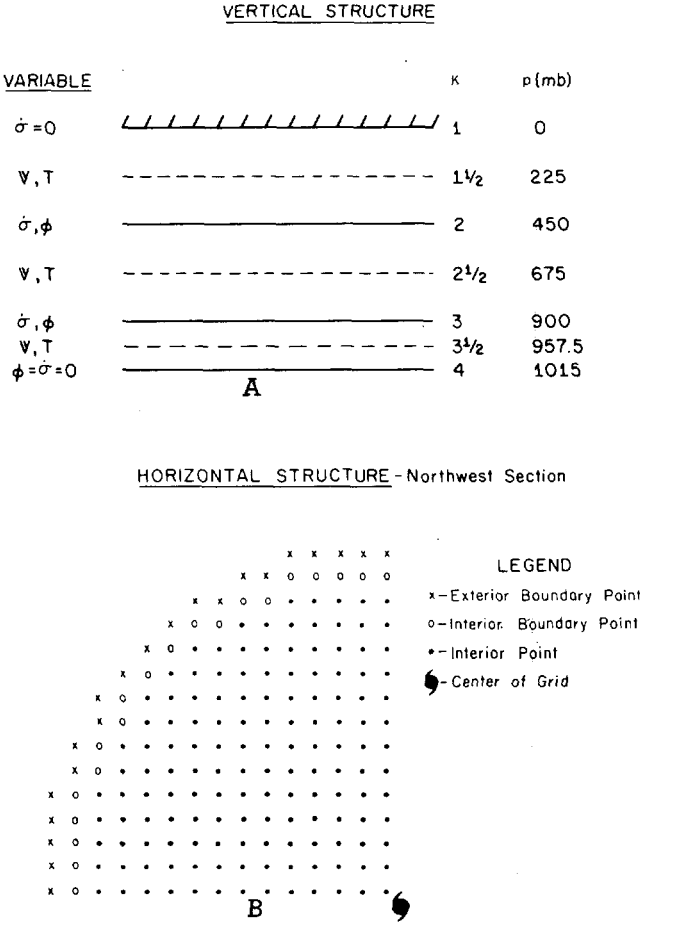

FIGURE 1.—(A) vertical information levels and (B) northwest quadrant of the horizontal grid.

C. THE FINITE-DIFFERENCE EQUATIONS

We adopt Shuman and Stackpole's (1968) finite-difference notation and write

$$\alpha_x\equiv\frac{\alpha_{i,j+1/2}-\alpha_{i,j-1/2}}{\Delta x},$$

$$\alpha_y\equiv\frac{\alpha_{i+1/2,j}-\alpha_{i-1/2,j}}{\Delta y},$$

$$\overline{\alpha}^x\equiv(\alpha_{i,j+1/2}+\alpha_{i,j-1/2})/2,$$

and (7)

$$\overline{\alpha}^y\equiv(\alpha_{i+1/2,j}+\alpha_{i-1/2,j})/2$$

where j is the east-west index and i is the north-south index. For vertical differences and averages, we define

$$\overline{\alpha}^\sigma\equiv(\alpha_{k+1/2}+\alpha_{k-1/2})/2$$

and (8)

$$\delta\alpha\equiv(\alpha_{k+1/2}-\alpha_{k-1/2}).$$

The horizontal portion of the difference scheme is similar to Grammeltvedt's (1969) scheme B and has been used extensively by the Geophysical Fluid Dynamics Laboratory, National Oceanic and Atmospheric Administration, in general circulation studies. With one exception, to be cited below, the vertical portion of the difference scheme has been discussed by Kurihara and Holloway (1967).

By use of the operators eq (7) and (8), the equations of motion can be expressed in the form

$$\frac{\partial p^*u}{\partial t}\approx-\overline{(up^*\overline{u}^x)}^x-\overline{(vp^*\overline{u}^y)}^y-p^*\frac{\delta(\dot{\sigma}\overline{u}^\sigma)}{\delta\sigma}-\overline{p^*\overline{\phi}^\sigma_x}^x-RT\overline{p^*}^x_x \quad (9)$$

and

$$\frac{\partial p^*v}{\partial t}\approx-\overline{(up^*\overline{v}^x)}^x-\overline{(vp^*\overline{v}^y)}^y-p^*\frac{\delta(\dot{\sigma}\overline{v}^\sigma)}{\delta\sigma}-\overline{p^*\overline{\phi}^\sigma_y}^y-RT\overline{p^*}^y_y \quad (10)$$

which are applied at the half levels. The continuity equation in the form

$$\frac{\partial p^*}{\partial t}=-[(\overline{u}^x\overline{p^*}^x)_x+(\overline{v}^y\overline{p^*}^y)_y]-p^*\frac{\delta\dot{\sigma}}{\delta\sigma} \tag{11}$$

is also applied at the half levels. The vertical sum of eq (11), subject to the boundary conditions $\dot{\sigma}=0$ at $\sigma=0$ and $\sigma=1$, is used to compute $\partial p^*/\partial t$. Equation (11) is then used to compute $\dot{\sigma}$ at the integral levels. The thermodynamic equation, also applied at the half levels, is written

$$\frac{\partial p^*T}{\partial t}=-[(\overline{p^*u}^x\overline{T}^x)_x+(\overline{p^*v}^y\overline{T}^y)_y]$$
$$-p^*\frac{\delta\dot{\sigma}\overline{T}^\sigma}{\delta\sigma}+\frac{RT\omega}{c_p\sigma}+\frac{p^*}{c_p}\dot{Q}+F_H(T). \tag{12}$$

The symbol, $\overline{T}^\sigma$, denotes a temperature at the integral levels computed by linear interpolation of *potential* temperature over σ between adjacent half levels. This provides for a substantial improvement in the calculation of static stability since potential temperature is much more nearly linear in σ than is temperature. Mintz and Arakawa (see Langlois and Kwok 1969) have adopted a similar procedure for their general circulation model.

The quantity $\omega=dp/dt$ is defined at the half levels and computed from

$$\omega=p^*\dot{\overline{\sigma}}^\sigma+\overline{\sigma}^\sigma\left(\frac{\partial p^*}{\partial t}+u\overline{p^*}^x_x+v\overline{p^*}^x_y\right). \tag{13}$$

The hydrostatic equation in the form

$$\frac{\delta\phi}{\delta\sigma}=-\frac{RT}{\overline{\sigma}^\sigma} \tag{14}$$

is also applied at the half levels.

With the exception of the use of $\overline{T}^\sigma$ in place of $\overline{T}^\sigma$ in the vertical flux terms of eq (12), the differencing and staggering of variables in the vertical is identical to that of Kurihara and Holloway (1967). For adiabatic inviscid flow in a laterally closed domain with $\dot{\sigma}=0$ at $\sigma=0$ and 1, Kurihara and Holloway showed their system to conserve the finite-difference analog to

$$\int_x\int_y\int_0^1 p^*\left(c_pT+\frac{u^2+v^2}{2}\right)d\sigma dydx. \tag{15}$$

It is clear that replacement of $\delta(\dot{\sigma}\overline{T}^\sigma)/\delta\sigma$ in the thermodynamic equation by $\delta(\dot{\sigma}\overline{T}^\sigma)/\delta\sigma$ will not alter the conservation of the integral eq (15) since either term will sum to zero given the boundary conditions on $\dot{\sigma}$ described above.

D. VERTICAL DIFFUSION OF MOMENTUM

Although vertical transport of horizontal momentum by the cumulus-scale motions has been shown to be an important element in maintaining the observed structure of hurricanes (Gray 1967, Rosenthal 1970*b*), this effect is not included in the preliminary calculations reported on here. Therefore, the terms $F_V(u)$ and $F_V(v)$ which appear in eq (1) and (2) represent, for this calculation, diffusive and "frictional" effects due to the vertical transports of horizontal momentum by subgrid eddies smaller than the cumulus scale. The most important aspect of these terms is the surface drag which produces frictional convergence in the cyclone boundary layer and, therefore, a water vapor supply which controls the parameterized cumulus convection (Charney and Eliassen 1964, Ooyama 1969, Rosenthal 1970*b*).

By use of vector notation, these terms may be written for the σ-system in the form

$$\mathbf{F}_V=-g\frac{\partial\boldsymbol{\tau}^z}{\partial\sigma} \tag{16}$$

where g is the acceleration of gravity and $\boldsymbol{\tau}^z$ is the vector Reynolds stress appropriate to the subcumulus eddies. To incorporate surface drag friction, we invoke the boundary condition

$$\tau^z_{k-\frac{1}{2}}=\rho^*C_D|\mathbf{V}^*|\mathbf{V}^* \tag{17}$$

where ρ^* is the density at the surface, C_D is a drag coefficient, and $\mathbf{V}^*$ is the surface wind.

Equation (17) is the well-known quadratic stress law. However, since winds are not defined at $\sigma=1$, eq (17) is approximated by

$$\tau^z_{k-\frac{1}{2}}=\rho^*C_D|\mathbf{V}_3|\mathbf{V}_3. \tag{18}$$

A value of 3×10^{-3} is adopted for C_D, and a standard value of 1.10 kg m^{-3} is used for ρ^* in eq (18). As an upper boundary condition, we require

$$\tau^z_{k-1}=0. \tag{19}$$

For the remaining σ-levels, we use the austausch formulation

$$\tau^z_{k-2,3}=\rho K(z)\frac{\partial\mathbf{V}}{\partial z}. \tag{20}$$

Here, ρ is density, z is height, and $K(z)$ is the kinematic coefficient of eddy viscosity. Following Smagorinsky et al. (1965), the Rossby-Montgomery formulation is adopted for $K(z)$,

$$K(z)=l^2\left|\frac{\partial\mathbf{V}}{\partial z}\right|, \tag{21}$$

where l is a mixing length given by

$$l=\begin{cases}k_0h\left(\dfrac{H-z}{H-h}\right), & h<z<H\\ 0, & z>H\end{cases}. \tag{22}$$

In these relationships, k_0 is the Kármán constant, h is the depth of the Prandtl layer, and H is the level at which the stress vanishes. We take $k_0=0.4$ and $h=100$ m.

If we consider the boundary condition eq (19), H should be identified with the $\sigma=0$ surface. To simplify matters, we allow l to vary linearly with σ. Thus,

$$l_k=k_0 h\sigma_k, \qquad k=1, 2, 3. \tag{23}$$

Finally, the finite-difference approximations for eq (20) and (21) are written

$$\tau^z=\bar{\rho}K(z)\frac{\delta \mathbf{V}}{\delta \bar{z}^\sigma} \tag{24}$$

and

$$K(z)=l^2\left|\frac{\delta \mathbf{V}}{\delta \bar{z}^\sigma}\right| \tag{25}$$

where $\bar{\rho}$ is an appropriate standard density for the given σ-surface. Both equations are applied at integral levels. The finite-difference expression for eq (16) then takes the simple form

$$\mathbf{F}_V=-g\frac{\delta \tau^z}{\delta \sigma}. \tag{26}$$

E. LATERAL MIXING TERMS

Following Smagorinsky et al. (1965), the lateral exchange of horizontal momentum by subgrid-scale eddies is written

$$F_H(\mathbf{V})=\frac{\partial}{\partial x}\left(K_H\frac{\partial p^*\mathbf{V}}{\partial x}\right)+\frac{\partial}{\partial y}\left(K_H\frac{\partial p^*\mathbf{V}}{\partial y}\right). \tag{27}$$

Preliminary tests, as well as calculations with a symmetrical analog to this model, revealed that neither a constant value of K_H nor Smagorinsky's (1965) variable K_H (proportional to the magnitude of the total deformation of the horizontal motion) provided acceptable results.

The formulation ultimately adopted was

$$K_H=C_1|\mathbf{V}|+C_2 \tag{28}$$

where $C_1=10^3$ m and $C_2=5\times10^3$ m^2 s^{-1}.

While this selection was based primarily on the results of numerical tests, the form was suggested by the encouraging results obtained from symmetrical models (Rosenthal 1970*b*, Yamasaki 1968*b*) which employed upstream differencing of advection terms with forward time steps. This scheme introduces a computational viscosity (Molenkamp 1968) which is similar to the variable portion of eq (28).

Although eq (28) is not very satisfying from a physical point of view, it does afford a useful interim representation of the statistical effect of horizontal interactions between the momentum fields of the cumuli and the macroscale. More satisfying formulations are dependent on the success of the future theoretical and observational studies of these interactions.

The preliminary tests also indicated that adequate results can be obtained if the lateral diffusion of heat is computed with a constant thermal diffusivity (K_T) of 5×10^4 m^2 s^{-1}. The lateral mixing term in the thermodynamic equation was, therefore, expressed in the form

$$F_H(T)=p^*K_T\left(\frac{\partial^2 T}{\partial x^2}+\frac{\partial^2 T}{\partial y^2}\right). \tag{29}$$

F. TIME INTEGRATION

A number of experiments were conducted for the purpose of selecting a method of time integration. Comparisons were made between the usual leapfrog method, the two-step Lax-Wendroff scheme (Richtmyer and Morton 1967), and the Matsuno (1966) simulated forward-backward scheme. With the diabatic and viscous terms suppressed, the Lax-Wendroff technique provided the best results from the point of view of preserving the finite-difference analog to the energy integral eq (15). The Matsuno method was almost as good (but at the cost of twice the computational time). The leapfrog method gave errors in the energy integral more than an order of magnitude greater than those encountered with the other methods.

On the other hand, with viscous and diabatic effects included, the Matsuno technique was clearly superior to the Lax-Wendroff technique. This conclusion was based on intuitive meteorological inspection of the test results. Presumably, the superiority of the Matsuno scheme is due to its severe damping of high temporal frequencies. Since this model has very limited vertical resolution, the high-frequency inertial gravity waves (particularly the external gravity wave) are probably overly excited by the diabatic heating. The Matsuno damping may, then, compensate for this effect.

Except for friction and heating, the scheme is summarized for the equation $\partial\alpha/\partial t = F(\alpha)$ as follows:

1. Given α^n.
2. $\alpha^* = \alpha^n + \Delta t F(\alpha^n)$.
3. Compute lateral boundary points from α^* data.
4. $\alpha^{n+1} = \alpha^n + \Delta t F(\alpha^*)$.
5. Compute lateral boundary points from α^{n+1} data.
6. Return to 1.

The superscript n refers to the time-step number, and Δt is 60 s. The friction and heating terms are computed using the α^n data in both steps 2 and 4. The extra time required by the two-step Matsuno scheme is only about 1.5 times that required by the other schemes tested.

G. LATERAL BOUNDARY CONDITIONS

The small domain size and the irregular boundary make the choice of lateral boundary conditions extremely important. Preliminary experimentation showed that realistic results could be obtained for steady-state pressure and temperature on the boundary and a variable momentum based on boundary conditions similar to those employed in symmetric models (Anthes 1970*a*; Rosenthal 1970*a*, 1970*b*).

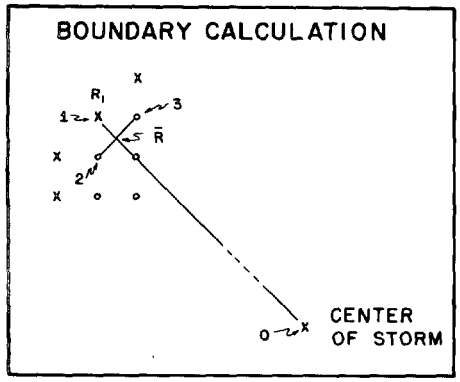

FIGURE 2.—Schematic diagram illustrating the calculation of lateral boundary point (1) based on interpolation between the nearest two interior points (2) and (3) and the boundary condition given by eq (30) in the text.

A sample calculation for a typical boundary point designated as number 1 in figure 2 is given below:

1. The vector velocity, $\mathbf{V}$, on the first two interior boundary points (2 and 3 in this example) is interpolated to the radius connecting the exterior boundary point (1) to the center of the storm (line 0–1). Let this mean velocity be designated as $\bar{\mathbf{V}}$ at radius $\bar{R}$ from the center.

2. The velocity, $\mathbf{V}_1$, at the exterior boundary point is then computed from

$$\mathbf{V}_1=\frac{\bar{R}}{R_1}\bar{\mathbf{V}}. \tag{30}$$

In the absence of azimuthal variations of $\mathbf{V}$, this condition [eq (30)] would correspond to the requirement that horizontal divergence and relative vorticity vanish at the boundary.

H. LATENT HEAT RELEASED IN ORGANIZED CUMULUS CONVECTION

As already noted, this preliminary experiment does not contain an explicit water cycle. Because of this, the convective adjustments of macroscale temperature are parameterized as they were in the original version of Rosenthal's (1969) symmetric model. The formulation contains ingredients suggested by previous investigators—in particular, Charney and Eliassen (1964), Kuo (1965), Ogura (1964), Ooyama (1969), Syōno and Yamasaki (1966), and Yamasaki (1968*a*, 1968*b*).

The basic characteristics of this convective adjustment are summarized as follows:

1. Convection occurs only in the presence of low-level convergence and conditional instability for air parcels rising from the surface.

2. All the water vapor that converges in the boundary layer rises in convective clouds, condenses, and falls out as precipitation.

3. All the latent heat thus released is made available to the macroscale flow.

4. The vertical distribution of this heating is such that the macroscale lapse rate is adjusted toward the pseudoadiabat appropriate to ascent from the surface.

Empirical justification for these characteristics is presented by Rosenthal (1969).

The heating function, previously written for the z-system (Rosenthal 1969), may be expressed in the σ-system as follows. Let

$$I=\frac{-L[(\nabla\cdot p^*\mathbf{V}q)\delta\sigma]_{k=7/2}}{\sum_{k=1}^{3}(T_c-T)_k\delta\sigma} \tag{31}$$

where T_c is the temperature along the pseudoadiabat with the equivalent potential temperature of the $\sigma=1$ surface, q is the specific humidity, and L is the latent heat of vaporization. Then,

$$p^*\dot{Q}=I(T_c-T) \tag{32}$$

if $I>0$ and $(\nabla\cdot p^*\mathbf{V}q)_{k=7/2}<0$.

Otherwise,

$$p^*\dot{Q}=0. \tag{33}$$

In finite-difference form,

$$(\nabla\cdot p^*\mathbf{V}q)_{k=7/2}=[(\overline{up^*q}^{x-x})_x+(\overline{vp^*q}^{y-y})_y]_{k=7/2}. \tag{34}$$

The convective adjustment defined by eq (32) applies only when the atmosphere is conditionally unstable ($T_c>T$). In mature hurricanes, however, prolonged and intense cumulus convection substantially reduces parcel buoyancy and lapse rates approach moist adiabatic values. Under these circumstances, significant amounts of nonconvective precipitation (and, hence, latent heat release) may occur (Hawkins and Rubsam 1968). Since, in this experiment, water vapor is not explicitly forecast, it is necessary to parameterize this effect.

The parameterization of nonconvective latent heat release under nearly moist adiabatic conditions proceeds as follows. Whenever $(T_c-T)\leq 0.5$°C at $k=3/2$ or 5/2, this quality is arbitrarily set to 0.5°C. Under a nearly moist adiabatic lapse rate, therefore, $T_c-T=0.5$°C at both levels, and the latent heat is partitioned equally between the upper and lower troposphere. From eq (32), therefore, latent heat is released in the column as long as a water vapor supply from the boundary layer is present.

The value of $q_{k=7/2}$, needed for the evaluation of eq (31), is assumed to be given by

$$q_{k=7/2}=\text{minimum}\left\{\begin{matrix}0.90q_s\\0.020\end{matrix}\right\}_{k=7/2} \tag{35}$$

where q_s is the saturation specific humidity. The upper bound of 0.020 imposed by eq (35) avoids excessive moisture values at points close to the storm center in the late stages of development when warm temperatures associated with an "eye" appear.[1]

[1] Empirical evidence (Sheets 1969) shows that q rarely exceeds 0.020 in mature hurricanes.

Finally, the surface humidity and temperature are required in order to establish the pseudoadiabat appropriate to parcel ascent from the surface. The surface temperature, T^*, is computed by a downward extrapolation from the temperature at level $k=7/2$,

$$T^*=T_{k=7/2}+3.636°\text{K}. \tag{36}$$

This corresponds to a lapse rate between the dry and moist adiabatic rates. The surface specific humidity, q^*, is obtained from $q_{k=7/2}$ through the assumption that the relative humidity is constant between the levels $k=7/2$ and $k=4$.

I. AIR-SEA EXCHANGE OF SENSIBLE HEAT

The sensible heat flux at the air-sea interface is assumed to obey the bulk aerodynamic relationship. It is further assumed that the heat flux decreases linearly with σ until it reaches a value of zero at the $k=3$ level. This gives

$$p^*\dot{Q}^s_{k=7/2}=\begin{cases}\dfrac{gc_p C_E|V|\rho^*(T_{sea}-T^*)}{\sigma_4-\sigma_3}, & T_{sea}>T^* \\ 0, & T_{sea}\leq T^*\end{cases} \tag{37}$$

where $\dot{Q}^s_{k=7/2}$ is the sensible heat added per unit mass and time at $k=7/2$. The exchange coefficient C_E is taken equal to C_D (0.003); $T_{sea}=302°$K is used for the experiment discussed below.

J. INITIAL CONDITIONS

The initial conditions consist of an axisymmetric vortex in gradient balance. These conditions are established as follows. The temperatures at the levels $k=3/2$, 5/2, and 7/2 are taken from a mean tropical atmosphere (Hebert and Jordan 1959). The initial surface pressure (in mb) is then defined by

$$p^*=1011.0-4.0\cos\left(\frac{\pi}{375}r\right), \quad r<375 \text{ km}$$

and

$$p^*=1015.0, \quad r\geq 375 \text{ km}$$

where r is given in kilometers.

The initial geopotentials of the σ-surfaces are calculated by an upward integration of the hydrostatic equation.

To obtain the initial wind field, we write the gradient wind equation for the σ-system

$$\frac{v_\lambda^2}{r}+fv_\lambda=\frac{RT}{p^*}\frac{\partial p^*}{\partial r}+\frac{\partial \phi}{\partial r} \tag{38}$$

where v_λ is the tangential wind component in cylindrical coordinates. Since the initial temperatures have no gradients on σ-surfaces, the second term on the right side of eq (38) gives no contribution. Thus, the only vertical variation present in the initial v_λ is due to the vertical variation of T in the (RT/p^*) $(\partial p^*/\partial r)$ term.

The pressure field eq (37) together with the specified temperature field yields a maximum gradient wind at the $k=7/2$ level of 18 m/s at a radius of 240 km. Although these conditions represent a rather strong vortex, experiments with the symmetric analog showed the mature state of the storm to depend very little on the strength of the initial vortex. The time of development, on the other hand, varied from 6 days to 1 day depending on the strength of the initial circulation. Therefore, a computational economy is realized by increasing the strength of the initial vortex.

To obtain initial values of u and v, the usual trigonometric relationships between velocity components in cylindrical and Cartesian coordinates were employed. In the absence of truncation and roundoff errors, the resulting u and v fields should be nondivergent and circularly symmetric. The truncation and roundoff errors as well as lack of complete circular symmetry in the boundary conditions do, however, produce weak asymmetries and divergences. Without these effects, the solution would remain circularly symmetric for all time.

3. EXPERIMENTAL RESULTS

The history of the cyclone is summarized by figure 3, which shows the evolution of the minimum surface pressure and the maximum wind speed in the boundary layer ($k=7/2$). Due to the substantial strength of the initial vortex, a short "organizational phase" of only 12 hr is needed before steady intensification begins. Hurricane-force winds appear at about 40 hr, and, thereafter, the relatively weak storm remains in a quasi-steady state until about 120 hr. At this point, a second period of intensification begins and the maximum wind eventually exceeds 60 m/s. The unsteady nature of the storm during this period seems to be related to the development of pronounced asymmetries (especially in the outflow region). The asymmetries are discussed in detail later.

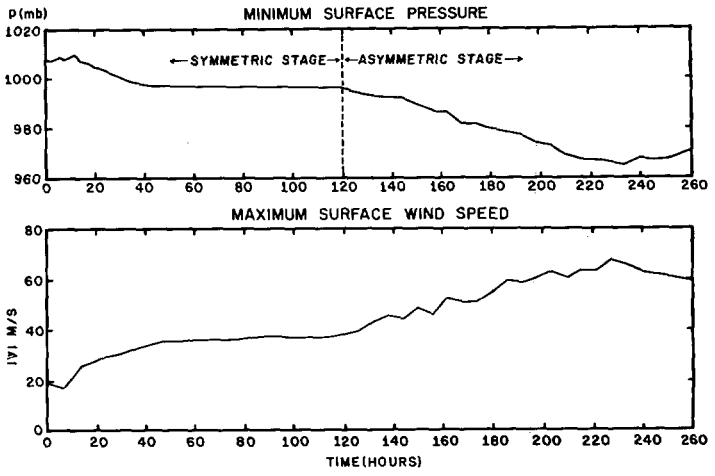

FIGURE 3.—Time variation of the minimum surface pressure and the maximum surface wind speed.

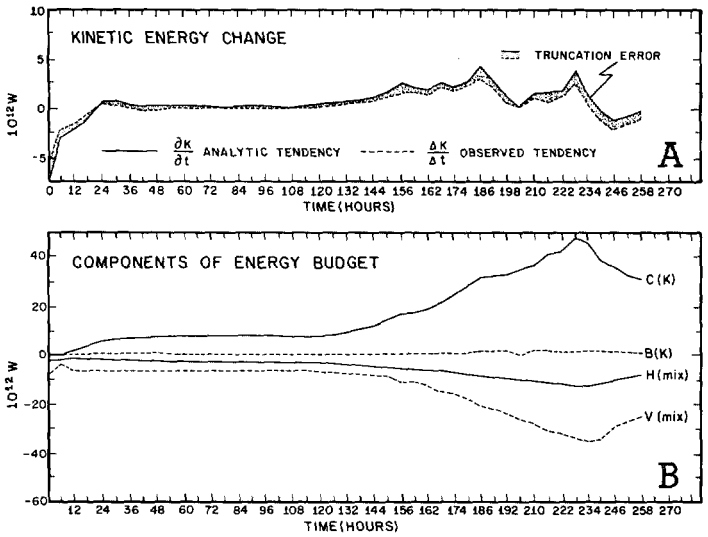

FIGURE 4.—(A) time variation of the observed kinetic energy change ($\Delta K/\Delta t$) and the change computed from the kinetic energy equation ($\partial K/\partial t$) and (B) time variation of individual components of the kinetic energy tendency. C(K) is the conversion of potential to kinetic energy, B(K) is the flow of kinetic energy through the lateral boundary, H(mix) is the loss of kinetic energy through lateral eddy viscosity and V(mix) is the loss of kinetic energy through vertical eddy viscosity including the effect of surface drag friction.

Figure 4B shows the temporal variations of the components of the kinetic energy budget. The sum of (1) the conversion of potential to kinetic energy [C(K)], (2) the flux of kinetic energy across the lateral boundary [B(K)], (3) the dissipation due to lateral mixing [H(mix)], and (4) the dissipation due to vertical mixing [V(mix)] equals the "analytic" kinetic energy tendency ($\partial K/\partial t$). Figure 4A shows the observed rates of change of kinetic energy ($\Delta K/\Delta t$). The difference between $\partial K/\partial t$ and $\Delta K/\Delta t$ is a measure of the truncation error and, as figure 4 shows, this difference is quite small. Furthermore, the individual components of the budget are reasonable when compared to empirical estimates (Hawkins and Rubsam 1968, Miller 1962, Palmén and Riehl 1957, Riehl and Malkus 1961).

For purposes of discussion, it is convenient to divide the history of the storm into two stages. From the initial instant until about 120 hr, all features are quite symmetric with respect to the storm center. During this period, there is neither evidence of a banded structure in the rainfall (analogous to rainbands in real hurricanes) nor does the upper tropospheric outflow show any preference for particular quadrants. We refer to this interval as the "early symmetric stage." After 120 hr, the upper outflow is quite asymmetric while the rainfall and vertical motions show distinct patterns analogous to the spiral rainbands found in real storms. We refer to this period as the "asymmetric stage." It is, however, important to keep in mind that these terms refer to the mesoscale features imbedded in the cyclone-scale vortex.

The life cycle of a tropical cyclone in the real atmosphere usually consists of three distinct phases. The first of these is commonly some type of wavelike disturbance in the easterlies or in the equatorial convergence zone. This "seedling" has a characteristic wavelength of 1000 km or so and, of course, is highly asymmetric when viewed from the synoptic scale. The model, in its present simple form, is unable to represent this early wave stage.

In the second phase of the life cycle of real storms, pressures decrease in some portion of the wave perturbation and a closed depression with a distinct, but weak, cyclonic circulation is formed. When viewed from the synoptic scale, this stage shows a much greater degree of circular symmetry than does the wave stage. While initial conditions for the model (a balanced symmetric vortex) are highly arbitrary, these are intended to be some sort of counterpart to this second stage of real storms. However, the first day or so of the calculation should really be thought of as an initialization rather than as a prediction. During this time, the initial conditions of gradient balance are modified toward a new slowly varying state in which divergence, friction, and diabatic heating are important elements.

As already noted, the term *early symmetric stage* as applied to the first 120 hr of the calculation refers to the symmetry of the imbedded mesoscale structure. This structure is in reasonable agreement with the mesostructure of the second stage of the life cycle of real storms as described above.

Finally, the real depression undergoes intensification to the mature stage. It is during this time that distinct rainbands are most likely to appear, thus producing pronounced asymmetries on the mesoscale. However, when viewed on the cylcone or synoptic scale, the mature stage may appear to be highly symmetric. There is, however, one major exception: The upper tropospheric outflow layer of the mature storm tends to be highly asymmetric even when viewed from the synoptic scale. The asymmetric stage of the model calculation is felt to be analogous to this mature stage of the real hurricane.

A. EARLY SYMMETRIC STAGE OF THE MODEL STORM

A representative view of the structure during this period is provided by the data at 84 hr. Figures 5 and 6 show the flow in the boundary layer (level 7/2) for this time. The region of hurricane-force winds is very small, extending only about 75 km from the center. Gale-force winds extend outward to 150 km. The maximum tangential and radial winds are 34.0 and −19.4 m/s, respectively, yielding an inflow angle of about 29°.

The circulation in the upper troposphere (level 3/2) shows a fairly symmetric outflow pattern (figs. 7 and 8). Cyclonic outflow occurs inside a radius of about 200 km. Beyond 200 km, the circulation is anticyclonic, reaching a maximum velocity of about 6 m/s around the outer boundary.

Dynamic (or inertial) instability of the upper tropospheric outflow has been suggested by Alaka (1961, 1962, 1963) and others as a contributory factor in the intensifica-

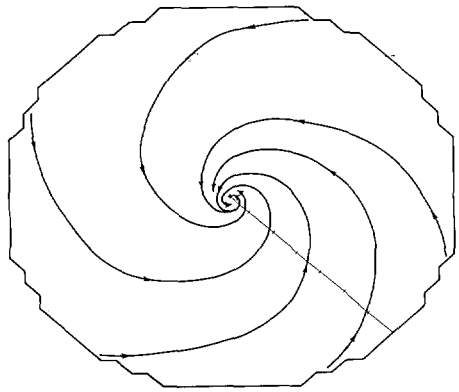

FIGURE 5.—Streamline analysis for the boundary layer (level 7/2) at 84 hr. Marks on the radial line from center of the grid to the lateral boundary represent 60-km intervals.

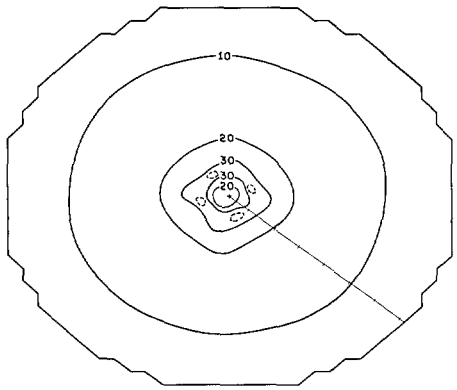

FIGURE 6.—Isotach analysis for the boundary layer (level 7/2) at 84 hr. Dashed contours near grid center represent 35-m/s isotachs. Isopleths are labeled in m/s.

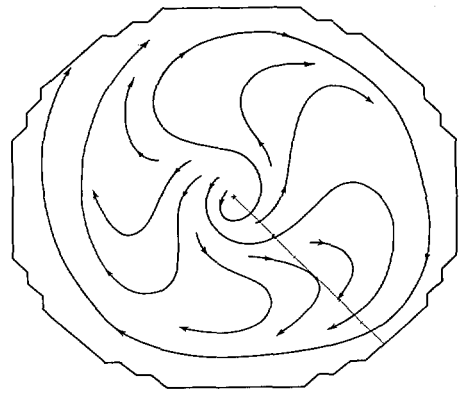

FIGURE 7.—Streamline analysis for the upper troposphere (level 3/2) at 84 hr.

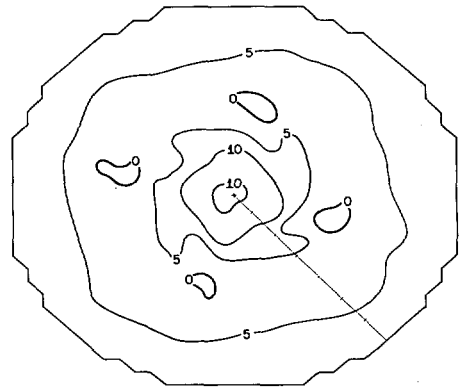

FIGURE 8.—Isotach analysis for the upper troposhere (level 3/2) at 84 hr. Contours labeled 0 contain wind speeds less than 0.5 m/s. Isopleths are labeled in m/s.

tion of tropical cyclones. An approximate necessary condition for this instability is given by

$$\zeta_a\left(\frac{2|\mathbf{V}|}{R}+f\right)<0 \tag{39}$$

where $|\mathbf{V}|$ is the wind speed, R is the radius of curvature of the streamlines, and ζ_a is the absolute vorticity. Condition (39) may be satisfied if either ζ_a or $[(2|\mathbf{V}|/R)+f]$ is negative. The second alternative corresponds to the occurrence of "anomalous" winds.

Great care must be taken in the application and interpretation of condition (39). Strictly speaking, this criterion for instability refers to horizontal parcel displacements normal to a streamline and is derived under the assumption that the velocity and pressure fields are invariant along the streamline. A necessary criterion for a closely related instability is

$$\left(\frac{\partial v_\lambda}{\partial r}+\frac{v_\lambda}{r}+f\right)\left(\frac{2v_\lambda}{r}+f\right)<0. \tag{40}$$

Criterion (40) concerns the instability of horizontal symmetric fluid-ring displacement in a symmetric vortex.

A third type of dynamic instability is governed by the necessary condition that the radial gradient of the absolute vorticity of the tangential flow have at least one zero. That is, the condition

$$\frac{\partial}{\partial r}\left(\frac{\partial v_\lambda}{\partial r}+\frac{v_\lambda}{r}+f\right)=0 \tag{41}$$

is satisfied somewhere in the fluid system. This is a necessary condition for asymmetric (azimuthally varying) horizontal perturbations to be unstable. The condition [eq (41)] can be derived in a straightforward manner by utilization of the techniques employed by Kuo (1949).

At the initial instant, when the flow is nearly symmetric and tangential, conditions (39) and (40) become equivalent. Since the initial data satisfy neither condition, these instabilities do not contribute to the very early intensification. On the other hand, eq (41) is satisfied even in the initial data since there is a maximum of cyclonic vorticity close to the center of the storm and a vorticity minimum (maximum of anticyclonic relative vorticity) at a radius of approximately 345 km. This should favor the growth of wavelike perturbations in the azimuthal direction. Since weak waves of this type are

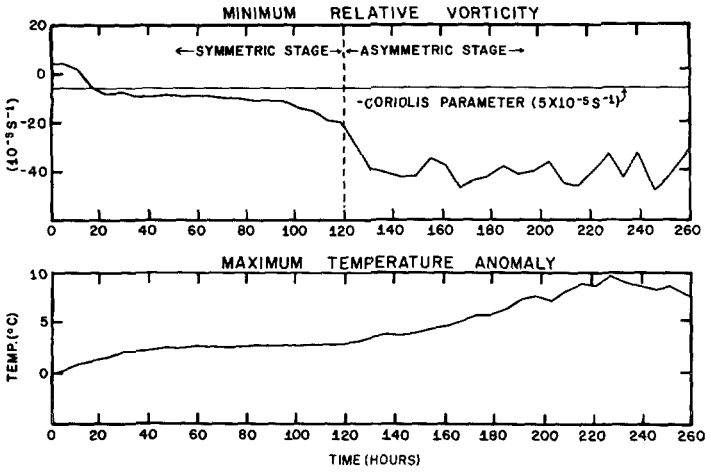

FIGURE 9.—(Top) time variation of the minimum relative vorticity in the upper troposphere (level 3/2) and (bottom) time variation of the maximum temperature anomaly (departure of temperature from the steady-state value at the lateral boundary) in the upper troposphere (level 3/2).

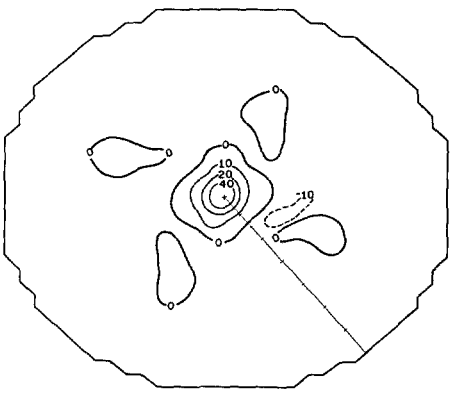

FIGURE 10.—Relative vorticity in the upper troposphere (level 3/2) at 84 hr. Isopleths are labeled in units of 10^{-5} s^{-1}.

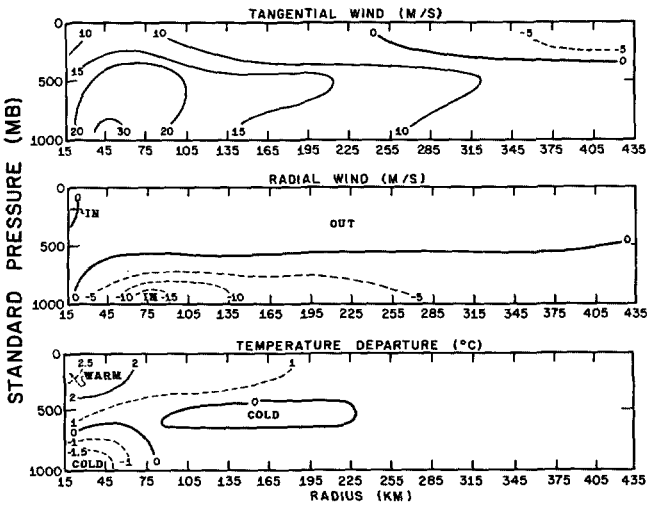

FIGURE 11.—Azimuthal mean vertical cross sections for the tangential wind, the radial wind, and the temperature anomaly at 84 hr. Isotherms are labeled in °C; isotachs are labeled in m/s.

already present in the initial data (see subsection 2J), and since, as already noted, substantial symmetry is retained for the first 120 hr, it is clear that the instability is either quite weak or that it is being counteracted by other effects such as those due to eddy viscosity.

Figure 9 (top) shows the time evolution of the minimum value of relative vorticity in the upper level within 350 km of the storm center. During the initial deepening stage, the minimum value of absolute vorticity becomes slightly negative. However, this occurs after the intensification and only over a small region.

Figure 10 shows the upper tropospheric relative vorticity at 84 hr, which is representative of the early symmetric stage. In view of the fact that the Coriolis parameter for this calculation is 5×10^{-5} s^{-1}, it is clear that only small patches of negative absolute vorticity are present. The term $[(2|\mathbf{V}|/R)+f]$ was also evaluated for several times during the first 120 hr. These calculations revealed only small patches of anomalous winds. We, therefore, also feel that the instabilities represented by conditions (39) and (40) played no significant role in the early symmetric stage of the model storm.

Azimuthally averaged vertical cross sections provide an adequate description of the storm structure during the early symmetric stage. Mean cross sections[2] of this type for the tangential wind, radial wind, and the temperature departure at 84 hr are shown in figure 11. These cross sections reveal a structure very typical of that of a weak hurricane (Hawkins and Rubsam 1968).

The pattern of temperature anomaly (departure from the steady-state temperature on the lateral boundary) shows a maximum positive anomaly of 2.8°C in the upper troposphere. This value is small compared to those found in mature hurricanes. For a weak hurricane, however, 2.8°C does not seem unreasonable for the average temperature of a deep upper tropospheric layer. The cold core at level 7/2 (due primarily to an excess of adiabatic cooling over sensible and latent heating) contributes significantly to the low tropospheric inward pressure-gradient force through the hydrostatic equation. Some preliminary experiments, in which the cold core did not appear, showed only slight intensification. It is noted that observations frequently show a cold lower troposphere in the early stages of storm development (Yanai 1961). There is also evidence for a low-level cold region in the mature stage (Hawkins and Rubsam 1968, Colón et al. 1961).

The vertical motion at the top of the boundary layer at 84 hr shows a nearly circular region of upward motion that extends from the center to about 180 km. Maximum velocities of about −140 mb/hr (about 0.4 m/s) occur in a ring near the center. Weak subsidence occurs in the

[2] The circular averages were computed by linear interpolation of grid point values to a polar grid with a radial increment of 30 km and an angular increment of 22.5°.

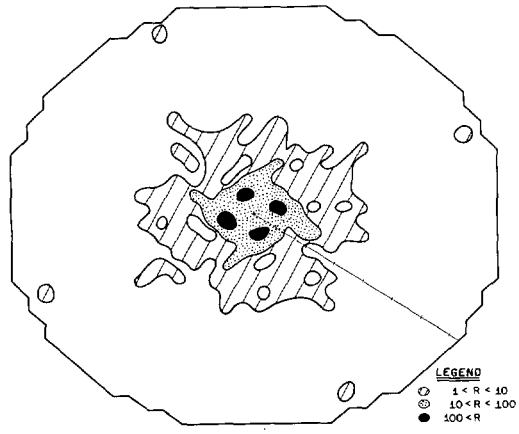

FIGURE 12.—Rainfall rates (cm/day) computed from the total latent heat release at 84 hr.

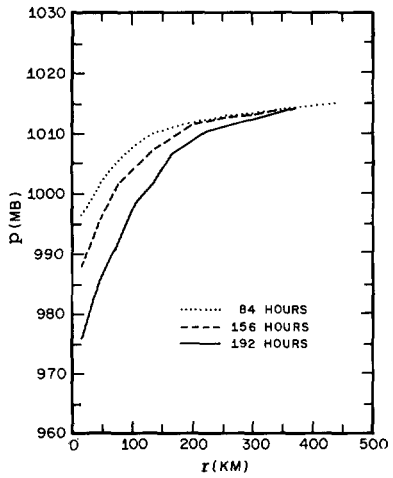

FIGURE 13.—Radial profiles of surface pressure along an east-west axis at 84, 156, and 192 hr.

environment beyond 180 km. The strongest upward velocities occur in the middle troposphere (level 5/2) and reach −230 mb/hr (about 0.7 m/s). These values appear reasonable for averages over a 30-km interval of a weak hurricane (Carlson and Sheets 1971).

Figure 12 shows the rainfall rates at 84 hr. These are computed by conversion of the total release of latent heat in a column to the equivalent liquid water depth. Values of over 100 cm/day occur locally near the center and decrease rapidly outward. The average rainfall over the inner 100 km is 65 cm/day which is comparable with the estimates made by Riehl and Malkus (1961) for hurricane Daisy (1958). The total release of latent heat at this time is 5.0×10^{14} W. This also compares favorably with empirical estimates (Anthes and Johnson 1968). Finally, the rainfall pattern at 84 hr shows no evidence of spiral bands.

Figure 13 shows surface pressure profiles for various times along one radius from the center of the grid. Since the surface isobars are very nearly circular, these profiles provide an adequate description of the surface pressure field. The minimum value at 84 hr (995 mb) is quite realistic for a maximum wind of 32 m/s (Colón 1963). The general shapes of the profiles agree well with observations (Fletcher 1955, Miller 1963).

The early symmetric period may be summarized as follows. After a short period of development (about 24 hr), a quasi-steady state is reached in which the model storm closely resembles a weak hurricane. The circulation is nearly axisymmetric. Air spirals inward in the low levels, ascends in a narrow ring, and flows outward in the upper levels. The outflow becomes anticyclonic beyond 200 km. However, the absolute vorticity in the outflow layer is positive except in small areas. The central pressure, temperature anomalies, rainfall rates, and the components of the kinetic energy budget correspond to a weak hurricane.

B. ASYMMETRIC STAGE OF THE MODEL

As shown by the central pressure, maximum wind speed, and maximum temperature anomaly (figs. 3 and 9), the storm begins a second period of intensification at about 120 hr. Figures 14 and 15 show the low-level streamline and isotach analyses at 156 hr. The inflow is still fairly symmetric, but shows an increased intensity over that at 84 hr. The maximum wind speed is now 46 m/s; hurricane-force winds extend outward to 80 km and gale-force winds to 210 km. The average angle of inflow has increased to 38°.

In contrast to the symmetric inflow, the outflow occurs in a highly asymmetric fashion (figs. 16 and 17). Outflow occurs in two quadrants, and several small eddies are located about the main center. This asymmetric nature of the outflow is typical of many hurricanes (e.g., Alaka 1961, 1962; Miller 1963).

The vorticity at level 3/2 shows large regions of negative absolute vorticity (fig. 18). This is in contrast with the vorticity pattern at 84 hr (fig. 10). These regions are transient. They form and re-form in various sectors of the outflow level. This unsteady behavior of the outflow is probably related closely to the oscillations in the central pressure and maximum surface wind during the latter portions of the computation (fig. 3). It is noted that negative absolute vorticity is an observed feature of hurricane outflow (Alaka 1962) and even appears as a feature of composite mean storms (Izawa 1964).

The presence of large values of negative absolute vorticity suggests the presence of one or more of the types of dynamic instability discussed in the previous subsection. Since condition (40) refers to symmetric instability and since eq (41) is satisfied in the initial data without noticeable effect, attention was focused on condition (39). The quantity, $2|\mathbf{V}|/R$, was computed for level 3/2 at 156 hr. In contrast to the early stages, anomalous winds are found to cover substantial areas of the domain and negative values of $2|\mathbf{V}|/R$ exceed 40×10^{-5} s^{-1} (fig. 19). The presence of anomalous winds in hurricane outflow

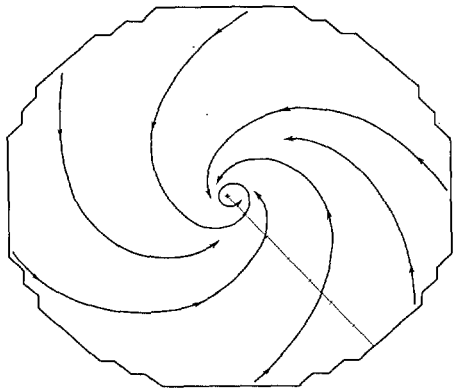

FIGURE 14.—Streamline analysis for the boundary layer (level 7/2) at 156 hr.

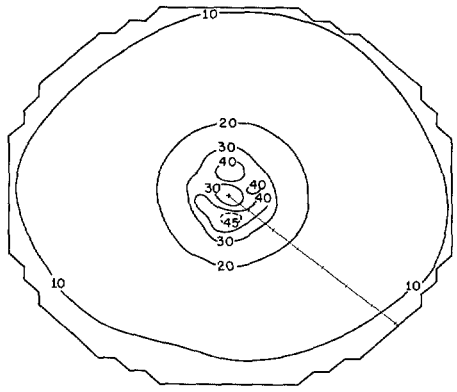

FIGURE 15.—Isotach analysis for the boundary layer (level 7/2) at 156 hr. Isopleths are labeled in m/s.

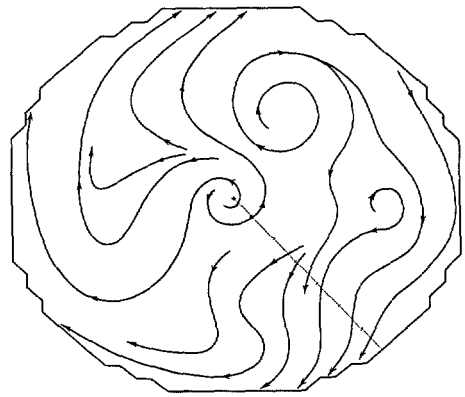

FIGURE 16.—Streamline analysis for the upper troposphere (level 3/2) at 156 hr.

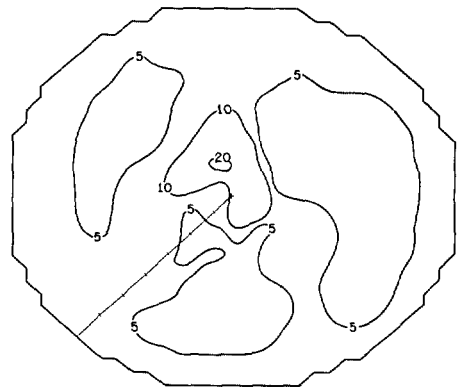

FIGURE 17.—Isotach analysis for the upper troposphere (level 3/2) at 156 hr. Isopleths are labeled in m/s.

has been documented by Alaka (1961). Indeed, the distribution and magnitude of $2|\mathbf{V}|/R$, as shown by figure 19, is in remarkable agreement with Alaka's calculation for the 35,000-ft level of hurricane Daisy (1958).

On the other hand, figure 19 also shows that the regions of anomalous winds are closely related to the regions of negative absolute vorticity. As a result, condition (39) is satisfied only in the stippled region shown on the figure. This result is also similar to Alaka's (1963) findings. The stippled region on figure 19 shows a great deal of similarity to the corresponding region in the outflow layer of 1958 hurricane Daisy [see fig. 3 in Alaka (1963)].

The role of dynamic instability in the development of tropical cyclones has been subjected to prolonged debate. The work of Alaka (1961, 1962, 1963) clearly demonstrates that condition (39) is satisfied in the outflow layers of hurricanes; Sawyer (1947) and Alaka (1963) have further suggested that dynamic instability must already be present before significant development can take place. The preexistence of dynamic instability in these hypotheses is accounted for by the presence of an upper tropospheric anticyclone. However, axisymmetric model calculations (Ooyama 1969, Rosenthal 1969) as well as the present asymmetric calculation indicate that dynamic instability

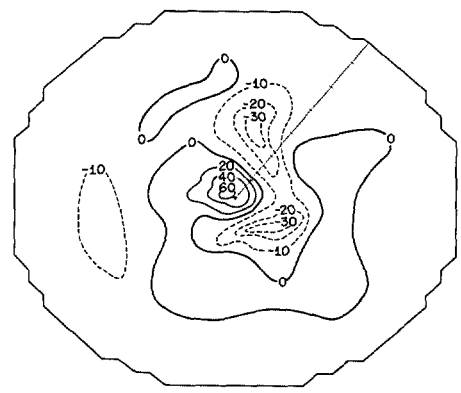

FIGURE 18.—Relative vorticity for the upper troposphere (level 3/2) at 156 hr. Isopleths are labeled in units of 10^{-5} s^{-1}.

is not a necessary condition for cyclone development, and instead can be generated as a consequence of cyclone intensification.

The numerical models, however, are probably not yet sufficiently sophisticated to give the final answer on this subject. In particular, all models available at this time consider only isolated vortexes and make no provision for interactions with surrounding synoptic systems. Further-

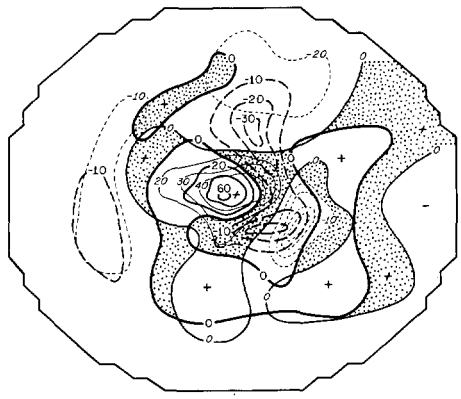

FIGURE 19.—Relative vorticity (heavy solid and dashed lines) and curvature term, $2|\mathbf{V}|/R$ (light solid and dashed lines), at 156 hr in the upper troposphere (level 3/2). The dotted area represents regions where the product of absolute vorticity and $2|\mathbf{V}|/R$ is negative. Isopleths are labeled in units of 10^{-5} s^{-1}.

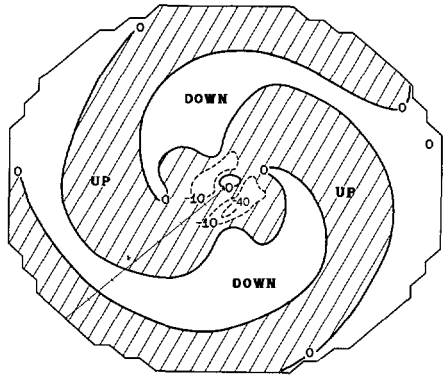

FIGURE 20.—Individual rate of change of pressure ($\omega = dp/dt$) for level 7/2 at 156 hr. Isopleths are labeled in units of cb/hr.

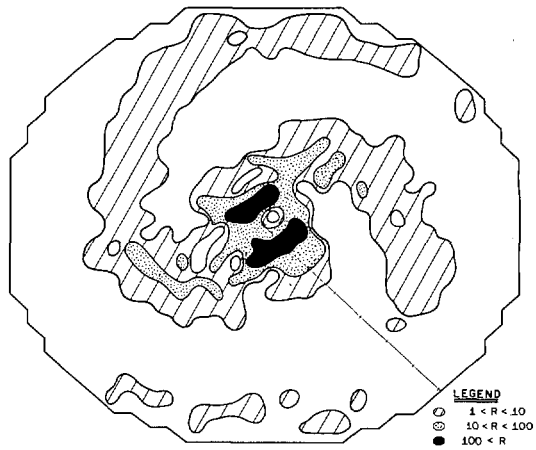

FIGURE 21.—Rainfall rates computed from the total release of latent heat at 156 hr. Isopleths are labeled in units of cm/day.

more, none of the models has, as yet, reached the stage where testing with real data is justifiable. Regardless of the situation in the real atmosphere, the second period of intensification in this model calculation appears to be related to the development of areas of dynamic instability. If we refer to figure 9, we note that the minimum vorticity in the outflow layer becomes suddenly more negative at about 100 hr. The second period of deepening (as measured by central pressure and maximum winds) *follows* this increase in negative absolute vorticity by about 20 hr (fig. 3). As we have already pointed out, this second period of deepening is accompanied by a breakdown of the symmetry which had prevailed during the first 120 hr of the calculation. Since it is well known that the release of dynamic instability does not directly provide new kinetic energy but transforms azimuthal mean kinetic energy into perturbation kinetic energy (Yanai 1964, Kuo 1962, Kasahara 1961), the change in structure of the model storm is consistent with the release of dynamic instability. The change in intensity may, in an indirect fashion, also be related to dynamic instability. The release of the dynamic instability provides for an increased upper level mass divergence and, therefore, increased low-level convergence. This, in turn, leads to a direct enhancement of the parameterized cumulus convection through eq (31) and (32). Coincident with the formation of asymmetries in the outflow is the appearance of spiral bands of rising motion which closely resemble hurricane rainbands. The vertical-motion pattern at level 7/2 (fig. 20) shows two bands of upward motion which begin at the edge of the domain and spiral inward toward the primary ring of upward motion near the center. The maximum vertical velocity near the center is −440 mb/hr (about 1.5 m/s).

In agreement with observations (Gentry 1964), the spiral bands are broken at a distance from the center (see the rainfall pattern, fig. 21) and become more solid as they spiral inward. The life span of a band is about 2.5 days.

The precipitation pattern, shown in figure 21, resembles a radar picture of a mature hurricane (e.g., Colón 1962, Colón et al. 1961, Donaldson and Atlas 1964). Strong convection occurs near the center in an irregular circle corresponding to an eye wall. Maximum rainfall rates in this region are over 100 cm/day. Two bands of weaker convection spiral in toward the center. The rainfall rates in the spiral bands are much less than those near the center of the storm, averaging only about 3 cm/day.

Tepper (1958) and Abdullah (1966) have suggested that hurricane rainbands are gravity waves similar to pressure jumps and, hence, to middle latitude squall lines. However, the rate of propagation and life span of these gravity waves (Abdullah 1966) are not at all consistent with the long life span of the observed bands (Gentry 1964) or those generated by the model. Faller (1962, 1965) has proposed that the rainbands may be explicable by Ekman-layer instability. The latter phenomenon has been reproduced in laboratory experiments with dishpans and results in spiral bands whose kinetic energy is derived from the kinetic energy of the mean tangential flow. This Ekman-

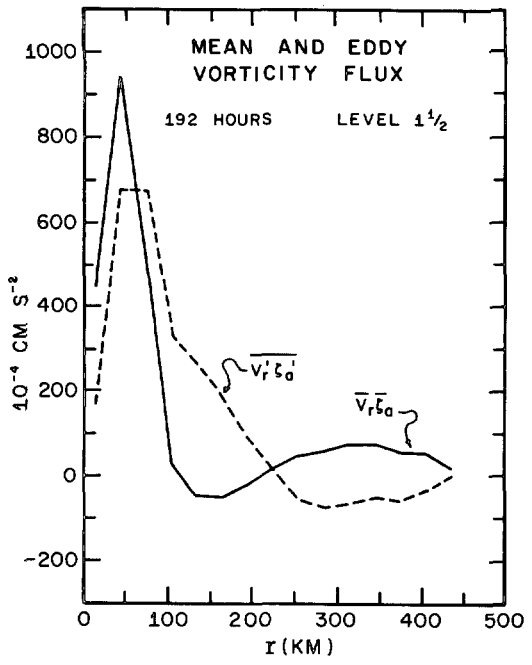

FIGURE 22.—Azimuthal mean ($\overline{v_r}^{\lambda}\overline{\zeta_a}^{\lambda}$) and eddy ($\overline{v_r'\zeta_a'}^{\lambda}$) horizontal vorticity flux in the upper troposphere (level 3/2) at 192 hr.

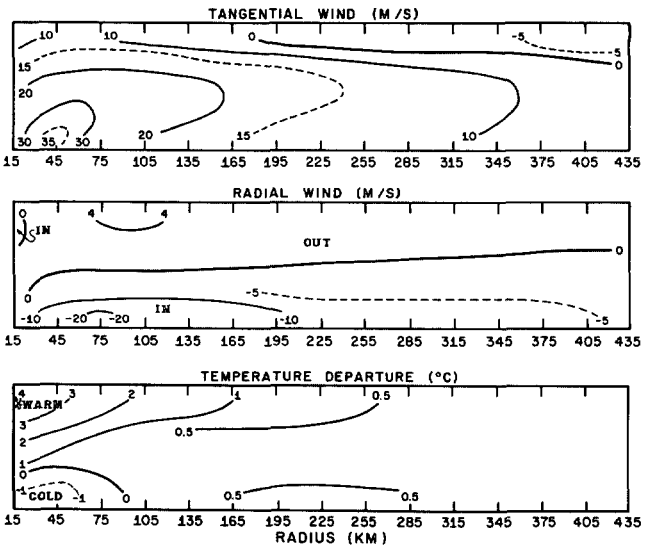

FIGURE 23.—Azimuthal mean vertical cross sections for the tangential wind, the radial wind, and the temperature anomaly at 156 hr. Isotherms are labeled in °C; isotachs are labeled in m/s.

layer instability may well contribute to the development of spiral bands in the real atmosphere as well as in the model calculation. However, the fact that the spiral bands do not appear in the model calculation until the symmetry of the outflow pattern has been destroyed suggests that the generation of the bands and the breakdown of the outflow pattern may be related. As we have noted above, the loss of symmetry in the outflow appears to be associated with dynamic instability. It should be emphasized, however, that this linkage is merely speculation at this time and will be pursued further when we have had the opportunity to perform experiments with greater horizontal resolution. Such experiments will allow meaningful budget calculations on the scale of the rainband.

In a recent paper, Anthes (1970*b*) hypothesized that large-scale asymmetries between radii of 400 and 1000 km from the hurricane center may play an important role in satisfying the angular momentum budget of the mature hurricane. The mean radial flux of vorticity may be written

$$A \equiv \overline{v_r'\zeta_a'}^{\lambda} + \overline{v_r}^{\lambda}\overline{\zeta_a}^{\lambda} \tag{42}$$

where the $\overline{(\ )}^{\lambda}$ operator refers to the azimuthal mean at a given radius and $(\ )'$ refers to departures from this mean.

For a hypothetical mean tangential velocity distribution which was typical of a hurricane, Anthes (1970*b*) calculated a minimum value of -150×10^{-4} cm·s^{-2} for the eddy term, $\overline{v_r'\zeta_a'}^{\lambda}$, in the upper troposphere at a radius of 400 km. This indicates that the outflow should be inversely correlated with absolute vorticity to satisfy the angular momentum budget in the slowly varying outflow region. Figure 22 shows the radial profiles of $\overline{v_r'\zeta_a'}^{\lambda}$ and $\overline{v_r}^{\lambda}\overline{\zeta_a}^{\lambda}$ computed for the model storm at 192 hr. Both mean and eddy transports of vorticity are positive inside 100 km. Beyond 100 km, however, where the vertical motion is small, there is indeed a negative correlation between outflow and absolute vorticity, and the eddy flux very nearly balances the mean flux from there to the limit of the domain.

Although the minimum value of $\overline{v_r'\zeta_a'}^{\lambda}$ in figure 22 is -70×10^{-4} cm·s^{-2} which is about half the minimum value found by Anthes (1970*b*), the qualitative agreement is good.

Figure 23 shows the azimuthally averaged vertical cross sections at 156 hr. The mean tangential and radial circulations are more intense than at 84 hr (fig. 11). The temperature section shows an increase in mean temperature anomaly from 2.5° to 4.1°C and a reduction in the low-level cold core maximum from −1.5° to −1.0°C. The weak middle-level cold region located between 105 and 225 km at 84 hr has disappeared by 156 hr.

In summary, beginning at about 100 hr, substantial areas of negative absolute vorticity appear in the upper level and the outflow pattern becomes asymmetric. Rainbands appear during this asymmetric stage. The storm is considerably less steady than during the earlier, symmetric stage, and the central pressure and maximum winds oscillate with a period of about 6 hr. This unsteady behavior appears to be related to the transient behavior of the regions of negative vorticity in the outflow layer.

From the time of appearance of the asymmetries at 120 hr, more or less continuous deepening occurs until

the storm reaches a maximum intensity at about 230 hr (fig. 3). At this time, the storm corresponds to a strong hurricane with a central pressure of 963 mb and a maximum wind speed of 65 m/s. The lapse rate in the inner region is very nearly pseudoadiabatic. After 230 hr, the storm begins to slowly fill and the calculation is terminated at 260 hr.

4. SUMMARY AND CONCLUSIONS

Preliminary results show that the model is capable of reproducing many observed features of the three-dimensional tropical cyclone. Rather realistic simulations of spiral rainbands and the strongly asymmetric structure of the outflow are obtained.

Despite a relatively coarse horizontal resolution of 30 km, the model produces a storm with maximum winds exceeding 65 m/s and a kinetic energy budget that compares favorably with empirical estimates.

In the mature asymmetric stage of the storm, substantial regions of negative absolute vorticity, anomalous winds, and dynamic instability are present in the upper troposphere. There is a suggestion that the breakdown of the early symmetry of the flow, as well as the deepening which takes place during the asymmetric stage, are related to the dynamic instability. Large-scale horizontal asymmetries in the outflow are found to play a significant role in the transport of vorticity during the mature stage. Beyond 200 km, the eddy transport of vorticity is opposite in sign and nearly equal in magnitude to the mean transport. This agrees well with earlier estimates.

Obvious deficiencies of the present model include the absence of a continuity equation for water vapor, the lack of a representation of the vertical transport of momentum by cumulus, a coarse horizontal resolution, and a small computational domain. Work toward the elimination of these shortcomings is in progress.

ACKNOWLEDGMENTS

The authors thank Mr. Billy M. Lewis for his cooperation in obtaining computer facilities for this experiment. We also thank the operators of the User 200 facility, Miss Shirley Parris, Mrs. Barbara Creech, Miss Deborah Goray, and Messrs. Karl Kellar and William Foltz for their time and effort that was necessary for the progress of the model.

We acknowledge Mr. Robert Carrodus, Mr. John Lundblad, and Mr. Glenn Frye for the drafting of the figures; and Mr. Charles True for the photography. We also thank Mrs. Mary Jane Clarke for typing the manuscript.

REFERENCES

Abdullah, Abdul Jabbar, "The Spiral Bands of a Hurricane: A Possible Dynamic Explanation," *Journal of the Atmospheric Sciences*, Vol. 23, No. 4, July **1966**, pp. 367–375.

Alaka, M. A., "The Occurrence of Anomalous Winds and Their Significance," *National Hurricane Research Project Report* No. 45, U.S. Department of Commerce, Weather Bureau, Miami, Fla., June **1961**, 26 pp.

Alaka, M. A., "On the Occurrence of Dynamic Instability in Incipient and Developing Hurricanes," *National Hurricane Research Project Report* No. 50, U.S. Department of Commerce, Weather Bureau, Miami, Fla., Mar. **1962**, pp. 51–56.

Alaka, M. A., "Instability Aspects of Hurricane Genesis," *National Hurricane Research Project Report* No. 64, U.S. Department of Commerce, Weather Bureau, Miami, Fla., June **1963**, 23 pp.

Anthes, Richard Allen, "A Diagnostic Model of the Tropical Cyclone in Isentropic Coordinates," *ESSA Technical Memorandum* ERLTM–NHRL 89, U.S. Department of Commerce, National Hurricane Research Laboratory, Miami, Fla., Apr. **1970a**, 147 pp.

Anthes, Richard Allen, "The Role of Large-Scale Asymmetries and Internal Mixing in Computing Meridional Circulations Associated With the Steady-State Hurricane," *Monthly Weather Review*, Vol. 98, No. 7, July **1970b**, pp. 521–528.

Anthes, Richard Allen, "Numerical Experiments With a Two-Dimensional Horizontal Variable Grid," *Monthly Weather Review*, Vol. 98, No. 11, Nov. **1970c**, pp. 810–822.

Anthes, Richard Allen, and Johnson, Donald R., "Generation of Available Potential Energy in Hurricane Hilda (1964)," *Monthly Weather Review*, Vol. 96, No. 5, May **1968**, pp. 291–302.

Carlson, Toby N., and Sheets, Robert C., "Comparison of Draft Scale Vertical Velocities Computed From Gust Probe and Conventional Data Collected by a DC–6 Aircraft," *ESSA Technical Memorandum* ERLTM–NHRL 91, U.S. Department of Commerce, National Hurricane Research Laboratory, Miami, Fla., June **1971**, 39 pp.

Charney, Jule G., and Eliassen, Arnt, "On the Growth of the Hurricane Depression," *Journal of the Atmospheric Sciences*, Vol. 21, No. 1, Jan. **1964**, pp. 68–75.

Colón, José A., "Changes in the Eye Properties During the Life Cycle of Tropical Hurricanes," *National Hurricane Research Project Report* No. 50, U.S. Department of Commerce, Weather Bureau, Miami, Fla., Mar. **1962**, pp. 341–354.

Colón, José A., "On the Evolution of the Wind Field During the Life Cycle of Tropical Cyclones," *National Hurricane Research Project Report* No. 65, U.S. Department of Commerce, Weather Bureau, Miami, Fla., Nov. **1963**, 36 pp.

Colón, José A., and Staff, "On the Structure of Hurricane Daisy," *National Hurricane Research Project Report* No. 48, U.S. Department of Commerce, Weather Bureau, Miami, Fla., Oct. **1961**, 102 pp.

Donaldson, Ralph J., Jr., and Atlas, David, "Radar in Tropical Meteorology: A Survey Paper," *Proceedings of the Symposium on Tropical Meteorology, Rotorua, New Zealand, November 5–13, 1963*, New Zealand Meteorological Service, Wellington, **1964**, pp. 423–473.

Faller, Alan J., "An Experimental Analogy to and Proposed Explanation of Hurricane Spiral Bands," *National Hurricane Research Project Report* No. 50, U.S. Department of Commerce, Weather Bureau, Miami, Fla., Mar. **1962**, pp. 307–313.

Faller, Alan J., "Large Eddies in the Atmospheric Boundary Layer and Their Possible Role in the Formation of Cloud Rows," *Journal of the Atmospheric Sciences*, Vol. 22, No. 2, Mar. **1965**, pp. 176–184.

Fletcher, Robert Dawson, "Computation of Maximum Surface Winds in Hurricanes," *Bulletin of the American Meteorological Society*, Vol. 36, No. 6, June **1955**, pp. 247–250.

Gentry, R. Cecil, "A Study of Hurricane Rainbands," *National Hurricane Research Project Report* No. 69, U.S. Department of Commerce, Weather Bureau, Miami, Fla., Mar. **1964**, 85 pp.

Grammeltvedt, Arne, "A Survey of Finite-Difference Schemes for the Primitive Equations for a Barotropic Fluid," *Monthly Weather Review*, Vol. 97, No. 5, May **1969**, pp. 384–404.

Gray, William M., "The Mutual Variation of Wind, Shear, and Baroclinicity in the Cumulus Convective Atmosphere of the Hurricane," *Monthly Weather Review*, Vol. 95, No. 2, Feb. **1967**, pp. 55–73.

Hawkins, Harry F., and Rubsam, Daryl T., "Hurricane Hilda, 1964: II. Structure and Budgets of the Hurricane on October 1, 1964," *Monthly Weather Review*, Vol. 96, No. 9, Sept. **1968**, pp. 617–636.

Hebert, Paul J., and Jordan, Charles L., "Mean Soundings for the Gulf of Mexico Area," *National Hurricane Research Project Report* No. 30, U.S. Department of Commerce, Weather Bureau, Miami, Fla., Apr. **1959**, 10 pp.

Izawa, Tatsuo, "On the Mean Wind Structure of Typhoon," *Typhoon Research Laboratory Technical Note* No. 2, Meteorological Research Institute, Tokyo, Japan, Mar. **1964**, 19 pp.

Kasahara, Akira, "A Study of the Stability of Thermally Driven and Frictionally Controlled Symmetric Motions With Application to the Mechanism for the Development of Tropical Cyclones," *Technical Report* No. 16, Contract No. Cwb–9941, Department of Meteorology, University of Chicago, Ill., Aug. **1961**, 63 pp.

Koss, Walter J., "Numerical Integration Experiments With Variable Resolution Two-Dimensional Cartesian Grids Using the Box Method," *Monthly Weather Review*, Vol. 99, No. 10, Oct. **1971**, pp. 725–738.

Kuo, Hsiao-Lan, "Dynamic Instability of Two-Dimensional Nondivergent Flow in a Barotropic Atmosphere," *Journal of Meteorology*, Vol. 6, No. 2, Apr. **1949**, pp. 105–122.

Kuo, Hsiao-Lan, "Mechanism Leading to Hurricane Formation," *National Hurricane Research Project Report* No. 50, U.S. Department of Commerce, Weather Bureau, Miami, Fla., Mar. **1962**, pp. 277–283.

Kuo, Hsiao-Lan, "On Formation and Intensification of Tropical Cyclones Through Latent Heat Release by Cumulus Convection," *Journal of the Atmospheric Sciences*, Vol. 22, No. 1, Jan. **1965**, pp. 40–63.

Kurihara, Yoshio, and Holloway, J. Leith, Jr., "Numerical Integration of a Nine-Level Global Primitive Equations Model Formulated by the Box Method," *Monthly Weather Review*, Vol. 95, No. 8 Aug. **1967**, pp. 509–530.

Langlois, W. E., and Kwok, H. C. W., "Description of the Mintz-Arakawa Numerical General Circulation Model," *Numerical Simulation of Weather and Climate, Technical Report* No. 3, Department of Meteorology, University of California, Los Angeles, Feb. **1969**, 95 pp.

Matsuno, Taroh, "Numerical Integrations of the Primitive Equations by a Simulated Backward Difference Method," *Journal of the Meteorological Society of Japan*, Ser. 2, Vol. 44, No. 1, Tokyo, Feb. **1966**, pp. 76–84.

Miller, Banner I., "On the Momentum and Energy Balance of Hurricane Helene (1958)," *National Hurricane Research Project Report* No. 53, U.S. Department of Commerce, Weather Bureau, Miami, Fla., Apr. **1962**, 19 pp.

Miller, Banner I., "On the Filling of Tropical Cyclones Over Land," *National Hurricane Research Project Report* No. 66, U.S. Department of Commerce, Weather Bureau, Miami, Fla., Dec. **1963**, 82 pp.

Molenkamp, Charles R., "Accuracy of Finite-Difference Methods Applied to the Advection Equation," *Journal of Applied Meteorology*, Vol. 7, No. 2, Apr. **1968**, pp. 160–167.

Ogura, Yoshimitsu, "Frictionally Controlled, Thermally Driven Circulations in a Circular Vortex With Application to Tropical Cyclones," *Journal of the Atmospheric Sciences*, Vol. 21, No. 6, Nov. **1964**, pp. 610–621.

Ooyama, Katsuyuki, "Numerical Simulation of the Life-Cycle of Tropical Cyclones," *Journal of the Atmospheric Sciences*, Vol. 26, No. 1, Jan. **1969**, pp. 3–40.

Palmén, Erik H., and Riehl, Herbert, "Budget of Angular Momentum and Kinetic Energy in Tropical Cyclones," *Journal of Meteorology*, Vol. 14, No. 2, Apr. **1957**, pp. 150–159.

Phillips, Norman A., "A Coordinate System Having Some Special Advantages for Numerical Forecasting," *Journal of Meteorology*, Vol. 14, No. 2, Apr. **1957**, pp. 184–185.

Richtmyer, Robert D., and Morton, K. W., *Difference Methods for Initial Value Problems*, 2d Edition, Interscience Publishers, New York, N.Y., **1967**, 405 pp.

Riehl, Herbert, and Malkus, Joanne S., "Some Aspects of Hurricane Daisy, 1958," *Tellus*, Vol. 13, No. 2, Stockholm, Sweden, May **1961**, pp. 181–213.

Rosenthal, Stanley L., "Numerical Experiments With a Multilevel Primitive Equation Model Designed to Simulate the Development of Tropical Cyclones: Experiment I," *ESSA Technical Memorandum* ERLTM–NHRL 82, U.S. Department of Commerce, National Hurricane Research Laboratory, Miami, Fla., Jan. **1969**, 36 pp.

Rosenthal, Stanley L., "A Survey of Experimental Results Obtained From a Numerical Model Designed to Simulate Tropical Cyclone Development," *ESSA Technical Memorandum* ERLTM–NHRL 88, U.S. Department of Commerce, National Hurricane Research Laboratory, Miami, Fla., Jan. **1970***a*, 78 pp.

Rosenthal, Stanley L., "A Circularly Symmetric Primitive Equation Model of Tropical Cyclone Development Containing an Explicit Water Vapor Cycle," *Monthly Weather Review*, Vol. 98, No. 9, Sept. **1970***b*, pp. 643–663.

Sawyer, John Stanley, "Notes on the Theory of Tropical Cyclones," *Quarterly Journal of the Royal Meteorological Society*, Vol. 73, Nos. 315–316, London, England, Jan.–Apr. **1947**, pp. 101–126.

Sheets, Robert C., "Some Mean Hurricane Soundings," *Journal of Applied Meteorology*, Vol. 8, No 1, Feb. **1969**, pp. 134–146.

Shuman, Frederick G., and Stackpole, John D., "Note on the Formulation of Finite Difference Equations Incorporating a Map Scale Factor," *Monthly Weather Review*, Vol. 96, No. 3, Mar. **1968**, pp. 157–161.

Smagorinsky, Joseph, Manabe, Syukuro, and Holloway, J. Leith, Jr., "Numerical Results From a Nine-Level General Circulation Model of the Atmosphere," *Monthly Weather Review*, Vol. 93, No. 12, Dec. **1965**, pp. 727–768.

Syōno, Sigekata, and Yamasaki, Masanori, "Stability of Symmetrical Motions Driven by Latent Heat Release by Cumulus Convection Under the Existence of Surface Friction," *Journal of the Meteorological Society of Japan*, Ser. 2, Vol. 44, No. 6, Tokyo, Dec. **1966**, pp. 353–375.

Tepper, Morris, "A Theoretical Model for Hurricane Radar Bands," *Proceedings of the Seventh Weather Radar Conference, Miami Beach, Florida, November 17–20, 1958*, American Meteorological Society, Boston, Mass., D c. **1958**, pp. K–56—K–65.

Yamasaki, Masanori, "A Tropical Cyclone Model With Parameterized Vertical Partition of Released Latent Heat," *Journal of the Meteorological Society of Japan*, Vol. 46, No. 3, Tokyo, June **1968***a*, pp. 202–214.

Yamasaki, Masanori, "Detailed Analysis of a Tropical Cyclone Simulated With a 13-Layer Model," *Papers in Meteorology and Geophysics*, Vol. 19, No. 4, Meteorological Research Institute, Tokyo, Japan, Dec. **1968***b*, pp. 559–585.

Yanai, Michio, "A Detailed Analysis of Typhoon Formation," *Journal of the Meteorological Society of Japan*, Ser. 2, Vol. 39, No. 4, Tokyo, Aug. **1961**, pp. 187–214.

Yanai, Michio, "Formation of Tropical Cyclones," *Reviews of Geophysics*, Vol. 2, No. 2, May **1964**, pp. 367–414.

[Received September 20, 1970; revised January 20, 1971]